NASA TN D-1716

TECHNICAL NOTE

D-1716

A DYNAMIC THERMAL VACUUM TECHNIQUE FOR MEASURING THE SOLAR ABSORPTANCE AND THERMAL EMITTANCE OF SPACECRAFT COATINGS

W. B. Fussell, J. J. Triolo, and J. H. Henninger
Goddard Space Flight Center
Greenbelt, Maryland

NATIONAL AERONAUTICS AND SPACE ADMINISTRATION
WASHINGTON
March 1963

A DYNAMIC THERMAL VACUUM TECHNIQUE FOR MEASURING THE SOLAR ABSORPTANCE AND THERMAL EMITTANCE OF SPACECRAFT COATINGS

by
W. B. Fussell, J. J. Triolo, and J. H. Henninger
Goddard Space Flight Center

SUMMARY

The various optical and thermal methods of measuring solar absorptance and thermal emittance are first discussed in some detail. Then the thermal vacuum technique used by Goddard Space Flight Center is described. The apparatus consists of: (1) a high vacuum chamber with inner walls cooled by liquid nitrogen, and (2) a powerful carbon arc lamp.

In operation a test sample coated with the material under investigation is suspended in the vacuum chamber facing a window in the chamber wall. A thermocouple in the test sample records its temperature. The sample is illuminated by the arc lamp, and its rise in temperature is recorded to above ambient temperature. While the arc lamp is *on*, its intensity of illumination is measured. The arc lamp is then turned *off*, and the sample's fall in temperature is recorded. From the sample's temperature-time data and the intensity of the arc lamp, the solar absorptance and thermal emittance can be computed to within ± 7 percent.

CONTENTS

A DYNAMIC THERMAL VACUUM TECHNIQUE FOR MEASURING THE SOLAR ABSORPTANCE AND THERMAL EMITTANCE OF SPACECRAFT COATINGS*

by
W. B. Fussell, J. J. Triolo, and J. H. Henninger†
Goddard Space Flight Center

INTRODUCTION

As shown by Hass, Drummeter, and Schach (Reference 1), the solar absorptance $\bar{a}$ and the thermal emittance $\bar{e}$ of spacecraft coatings are of fundamental importance in determining the equilibrium temperature of a satellite in space: The input term in the radiation balance equation of a satellite is proportional to the solar absorptance, and the output term is proportional to the thermal emittance. (Several other factors, such as the solar illumination intensity, the satellite orientation, etc., of course enter into the radiation equation.)

There are a number of different methods of measuring $\bar{a}$ and $\bar{e}$. One way of classifying these methods is by the type and variety of data obtained. Optical methods measure $\bar{a}$ and $\bar{e}$ by the radiation reflected from, or emitted by, materials; this radiation may be either spectrally resolved or integrated. Thermal methods measure $\bar{a}$ and $\bar{e}$ by the temperature or rate of temperature change of materials. Optical methods require the elimination of, or the control of, background radiation. Thermal methods require, in addition, the evacuation to high vacuum of the chamber surrounding the material sample being measured. Also, to obtain $\bar{a}$ values by thermal methods, a light source whose spectral distribution is similar to that of the sun *(solar simulator)* is necessary, plus instrumentation for measuring the intensity of the light from the solar simulator.

This report will first classify the various optical and thermal methods of measuring $\bar{a}$ and $\bar{e}$; and discuss the instrumentation available, each method's advantages and disadvantages, and the accuracy and validity – from the thermal design viewpoint–of the data obtained. Finally, the thermal vacuum technique used by Goddard Space Flight Center, as well as the equipment and operating procedure, will be described in detail. The accuracy and validity of the results, and the data reduction procedure, will be discussed.

*Presented at the Symposium on Measurement of Thermal Radiation Properties of Solids, Dayton, Ohio, Sept. 5, 1962. To be published in Proceedings.

†American Research and Manufacturing Corporation, Rockville, Md.

METHODS FOR MEASURING $\bar{a}$ AND $\bar{e}$

The different methods for measuring $\bar{a}$ and $\bar{e}$ can be classified as follows:

A. Optical methods
   1. Reflectance measurements
      a. Spectrally resolved
         (1) 0.3 to 2.5 microns, for $\bar{a}$
         (2) 5 to 35 microns, for $\bar{e}$
      b. Integrated
         (1) Light source times detector response must match solar spectrum approx., for $\bar{a}$
         (2) Light source times detector response match 300° K blackbody approx., for $\bar{e}$
   2. Emitted radiation measurements (for $\bar{e}$ only)
      a. Spectrally resolved, 5 to 35 microns
      b. Integrated

B. Thermal methods
   1. Equilibrium measurements
      a. With electrical heating, for $\bar{e}$
      b. With solar simulator as heater, for $\bar{a}$ and $\bar{e}$
      c. With solar simulator as heater (water calorimeter), for $\bar{a}$
   2. Dynamic measurements
      a. With solar simulator as heater, for $\bar{a}$ and $\bar{e}$
      b. Adiabatic cooling, for $\bar{e}$

The above methods will be discussed in sequence, as well as the instrumentation available, each method's advantages and disadvantages, and the accuracy and validity – from the thermal design viewpoint – of the data obtained.

Optical Methods

Spectrally Resolved Reflectance Measurements from 0.3 to 2.5 microns, for $\bar{a}$ [A1a(1)]

This wavelength region contains 95.3 percent of the sun's energy (Reference 2), 1.2 percent below 0.3 micron and 3.4 percent above 2.5 microns. Total reflectance measurements can be made to a precision of ±0.5 percent absolute (e.g., a reading of 11 percent reflectance lies between 11.5 and 10.5 percent) with a Beckman DK-2 Spectrophotometer having an integrating sphere reflectance attachment. However, the integrating sphere is most accurate when the test sample reflectance is near that of the reflectance standard used and when the polar reflectance patterns are similar (Reference 3).

Thus a specular sample should be measured with a specular standard, and a diffuse sample with a diffuse standard. If the test sample is neither perfectly diffuse nor perfectly specular, but falls somewhere in between, it may be difficult to obtain a reflectance standard having a similar polar reflectance pattern. In this case the accuracy of the measurement may be questionable, since the average number of reflections undergone by light reflected from the test sample before it reaches the detector may not be equal to the average number of reflections undergone by light reflected from the reflectance standard. If the interior coating of the sphere possessed a reflectance of 100 percent, this difference in the average number of reflections would be unimportant, since it is the light *absorbed* at each reflection that produces a difference between measurements otherwise equal but having a different average number of reflections. The highest reflectance obtainable for a sphere coating at present is about 98 percent (in the visible) with a thick (several millimeters) coating of magnesium oxide, and so there is a possibility of error in reflectance measurements with an integrating sphere on materials having both a diffuse and specular component of reflectance. Unfortunately there is not at present a good theoretical treatment of the integrating sphere when used with materials of this type, and the magnitude of the error for these materials is difficult to estimate.

Since solar illumination will usually strike the exterior surface of a satellite at both normal and non-normal incidence, it is important to know the variation of the solar absorptance of a material with angle of incidence. If the optical constants n and k (n being the index of refraction, and k the extinction coefficient) of the material are known at a reasonable number of wavelengths in the 0.3 to 2.5 micron range, then Fresnel's equations (Reference 4, p. 531) enable its solar absorptance to be computed at any angle of incidence. It is also possible to compute the solar absorptance of a material at a given incidence angle from its total reflectance spectrum obtained experimentally. Although the conventional integrating sphere reflectometer gives the total reflectance for normal, or near-normal, illumination only (a quantity called the *total normal reflectance*), a modified design of integrating sphere that allows total reflectance to be measured at angles of incidence from 10 to 80 degrees has been made.*

Mathematically expressed, the procedure for computing the solar absorptance of a given material from its total reflectance spectrum at a given angle of incidence is:

$$\bar{a}(\theta) = 1 - \bar{\rho}(\theta) , \tag{1}$$

$$\bar{\rho}(\theta) = \frac{\int_{\lambda = 0.3\mu}^{\lambda = 2.5\mu} R_\lambda(\theta) H_\lambda \, d\lambda}{\int_{\lambda = 0.3\mu}^{\lambda = 2.5\mu} H_\lambda \, d\lambda} ; \tag{2}$$

where

$\bar{a}(\theta)$ = solar absorptance at angle of incidence θ,

$R_\lambda(\theta)$ = total reflectance at wavelength λ at θ,

*This equipment can be obtained from Gier and Dunkle, Thermal Instruments, Los Angeles 66, Calif.

H_λ = solar extraterrestrial spectrum (Reference 2),

$\bar{\rho}(\theta)$ = solar reflectance at θ.

In practice, the integrals in Equation 2 are approximated by discrete summations.

An experienced technician can measure a sample's total normal reflectance spectrum through the solar region on a conventional recording integrating sphere spectroreflectometer and can compute its normal solar absorptance in approximately 2 hours, using manual read-off and data reduction techniques. Digital read-out and computer data integration would reduce this time drastically.

Spectrally Resolved Reflectance Measurements from 5 to 35 microns, for $\bar{e}$ [*A 1 a(2)*]

This wavelength interval contains 91.0 percent of the energy of a 300° K blackbody, 1.3 percent of its energy being radiated at shorter wavelengths and 7.7 percent at longer wavelengths (using for C_2, the second radiation constant in Planck's function, the value 1.438 cm-°K). Total reflectance measurements can be made in this region by a "hohlraum" (heated oven) attachment to an infrared spectrophotometer* or by a "Coblentz" hemispherical mirror attachment to an infrared spectrophotometer.† The heated oven has two openings, one of which allows the insertion of a water-cooled sample holder that keeps the sample at a reasonable temperature (100° F) even though the oven may be very hot (1100° C). The other opening allows the infrared spectrophotometer to view either the interior wall of the oven or the sample, and thus acts as the radiation source for the spectrophotometer. The Coblentz hemisphere is really an approximation to an ellipsoidal mirror and is based on the light-collecting properties of such a mirror, all light reflected from a sample placed at one focus of the ellipsoid being collected by the mirror and brought to a focus at the conjugate focus of the mirror. Thus an infrared detector placed at the conjugate focus will respond to the reflected light from the sample. If the *field-of-view* of the detector is wide enough to encompass a complete hemisphere, the detector will measure the sample total reflectance (provided also the detector has uniform spatial sensitivity).

The hohlraum oven can be used to make either absolute or relative total reflectance measurements. The interior wall of the oven is approximately an isothermal blackbody and provides in this manner an absolute standard of radiation‡ against which the reflected light from the sample can be compared. It is also possible to use the hohlraum oven for relative reflectance measurements by making two runs: one giving the sample reflectance relative to the oven, and the other giving the reflectance of a standard whose absolute reflectance is known relative to the oven.

By the principle of reciprocity (Reference 4, p. 208) it can be shown that the total reflectance of a material illuminated at a given angle of incidence, as measured by an integrating sphere or collecting mirror, is equal to the total reflectance of the material under conditions of *uniform* diffuse

*E.g., a Perkins-Elmer Model 13 Infrared Spectrophotometer in conjunction with a Model 205 Diffuse Reflectance Attachment (made by Perkins-Elmer Corp., Norwalk, Conn.).

†E.g., a Beckman Hemisphere Reflectance Attachment used in conjunction with an IR-7 Infrared Spectrophotometer (made by Beckman Instruments, Inc., Fullerton, Calif.).

‡The fundamental requirement here is that the wall of the oven be at least spatially uniform in the sense of having a uniform brightness - at each wavelength of measurement - when viewed from any direction.

illumination – the reflected light now being viewed by a detector at an angle equal to the angle of incidence. The essence of proof of this statement is the reciprocity of the transfer function, denoted by $\tau(\theta, \theta')$, which describes the amount of light incident at an angle θ (from a small element of solid angle dw) that is scattered into a small element of solid angle about the angle of reflection θ. (For simplicity, the transfer function is assumed not to depend on the azimuthal angle ψ; the proof still holds even if τ is a function of ψ.) The principle of reciprocity is that

$$\tau(\theta, \theta') = \tau(\theta', \theta) .$$

The measurement and data reduction procedures for computing the total hemispherical emittance and the total normal emittance of a material are expressed concisely by the following equations:

$$\bar{e}_H(T) = \bar{a}_H(T) , \tag{3}$$

$$\bar{a}_H(T) = 1 - \rho_H(T) , \tag{4}$$

$$\bar{\rho}_H(T) = \frac{\int_{\lambda = 5\mu}^{\lambda = 35\mu} \int_{\theta = 0}^{\theta = \pi/2} \rho(\theta, \lambda) 2\pi \sin\theta \cos\theta \, d\theta J_\lambda(T) \, d\lambda}{\int_{\lambda = 5\mu}^{\lambda = 35\mu} \int_{\theta = 0}^{\theta = \pi/2} 2\pi \sin\theta \cos\theta \, d\theta J_\lambda(T) \, d\lambda} , \tag{5}$$

$$\bar{e}_N(T) = \bar{a}_N(T) , \tag{6}$$

$$\bar{a}_N(T) = 1 - \bar{\rho}_N(T) , \tag{7}$$

$$\bar{\rho}_N(T) = \frac{\int_{\lambda = 5\mu}^{\lambda = 35\mu} \rho_N(\lambda) J_\lambda(T) \, d\lambda}{\int_{\lambda = 5\mu}^{\lambda = 35\mu} J_\lambda(T) \, d\lambda} ; \tag{8}$$

where

$\bar{e}_H(T)$ = total hemispherical emittance at temperature T (degrees absolute),

$\bar{a}_H(T)$ = total hemispherical absorptance for radiation of temperature T [by Kirchoff's law of radiation (Reference 4, p. 429), $\bar{e}_H(T)$ and $\bar{a}_H(T)$ are equal],

$\bar{\rho}_H(T)$ = total hemispherical reflectance for radiation of temperature T,

$\rho(\theta, \lambda)$ = total reflectance for illumination incident at the angle θ and the wavelength λ,

$J_\lambda(T)$ = Planck blackbody function for the total radiation normal to the radiating surface of blackbody per unit area, per unit solid angle, and per unit wavelength interval at T and λ:

$$J_\lambda = C_1' \left[\lambda^5 \exp\left(\frac{C_2}{\lambda_T}\right) - 1 \right]^{-1}$$

with $C_1' = 1.191 \times 10^{-5}$ erg-cm^2/sec and $C_2 = 1.439$ cm-°K,

$\bar{e}_N(T)$ = total normal emittance at T,

$\bar{a}_N(T)$ = total normal absorptance at T [$\bar{a}_N(T) = \bar{e}_N(T)$ by Kirchoff's law of radiation, as noted above],

$\bar{\rho}_N(T)$ = total normal reflectance at T.

In the actual computations, of course, the integrals in Equations 5 and 8 are replaced by discrete summations. In the hohlraum oven reflectometer and the Coblentz hemisphere reflectometer described above, the quantity measured is $\rho(0, \lambda)$ the total *normal* reflectance at wavelength λ. A variable angle of incidence hohlraum oven can be obtained commercially, however, and allows values of $\rho(\theta, \lambda)$ to be obtained over the range from θ = 20 to 70 degrees.

If experimental data on $\rho(\theta, \lambda)$ are lacking and only data for $\rho(0, \lambda)$ are available, the integration indicated in Equation 5 with respect to θ can be carried out by using the theoretical variation of $\rho(\theta, \lambda)$ with θ. Details of this procedure are given in Jakob's work on heat transfer (Reference 5, pp. 41-52). The process consists, basically, of assuming the test material to be an isotropic substance with known optical constants and with a smooth flat surface. In this case Fresnel's equations (Reference 4, p. 531) can be used – as mentioned previously — to calculate the reflectance $\rho(\theta, \lambda)$ for any θ at any λ for which the optical constants are known. Since smooth surfaces are required by the theory, this excludes roughened and diffusely reflecting surfaces. Jakob presents tables and graphs (Reference 5, pp. 43, 51, and 52) giving the ratio of total hemispheric emissivity to total normal emissivity as a function of total normal emissivity for electrical conductors and insulators. By means of these data, values of total normal emittance obtained from optical measurements can be converted to total hemispherical emittance, the quantity of interest for thermal design purposes.

An experienced technician using a conventional infrared recording spectrophotometer, attached to a hohlraum oven as described above for its radiation source, can measure the total reflectance spectrum of a sample over the thermal region and can read off and reduce the data manually to a total normal emittance value in approximately 1 to 1-1/2 days.

Integrated (Nonspectrally Resolved) Reflectance Measurements over the Solar Spectrum, for $\bar{a}$ [*A 1 b(1)*]

If a light source and a detector combination can be found whose combined response function matches the solar spectrum approximately (such a device should not be difficult to construct), then this source-detector combination could be used with an integrating sphere or collecting mirror total reflectometer to give solar absorptance values for materials directly. For many common spacecraft coatings (e.g., aluminum, gold, silver, black and white paints), the spectral match between the light source – detector response function and the solar spectrum need not be particularly close on a high resolution basis. The important thing is that the average absorptance for the light source – detector spectrum should be close to the average absorptance for the solar spectrum. That is,

$$\bar{a} = \frac{\int_{\lambda = 0.3\mu}^{\lambda = 2.5\mu} a_\lambda H_\lambda \, d\lambda}{\int_{\lambda = 0.3\mu}^{\lambda = 2.5\mu} H_\lambda \, d\lambda} , \qquad (9)$$

the solar absorptance, should be approximately equal to

$$\bar{a}' = \frac{\int_{\lambda = 0.3\mu}^{\lambda = 2.5\mu} a_\lambda S_\lambda \, d\lambda}{\int_{\lambda = 0.3\mu}^{\lambda = 2.5\mu} S_\lambda \, d\lambda}, \tag{10}$$

the average absorptance for the light source – detector spectrum, where a_λ is the absorptance at λ and S_λ is the source-detector spectral intensity at λ.

Practically, it seems that an incandescent lamp with a suitable filter and a flat thermal detector such as a bolometer or thermopile might work. Possibly an incandescent lamp in conjunction with a phototube having an S-1 response would be acceptable. It is known* that a carbon arc with rare-earth cored carbons is a good solar simulator in the above sense.

Integrated Reflectance Measurements over the Thermal (300° K) Spectrum, for $\bar{e}$ [A 1 b(2)]

If a radiation source – detector combination whose combined response function matches the spectrum of approximately a 300° K blackbody can be found, this source-detector combination could be used with a collecting mirror total reflectometer to give thermal emittance values for materials directly. The hohlraum oven reflectometer used in conjunction with a flat thermal detector would obviously need filtering if operated in its normal temperature range (800° to 1000° C).

It is possible that chopped blackbody radiation at 50° to 100° C above ambient temperature, if efficiently collected by suitable optics (at least f/2, say), would provide sufficient power to measure thermal emittance with a thermopile in the above manner (this assumes a thermopile with a responsivity of 0.1 volt/watt, a receiver area of 1 mm², and a minimum output of 10 microvolts).

Spectrally Resolved Emitted Radiation Measurements from 5 to 35 microns, for $\bar{e}$ (A 2 a)

The thermal radiant power emitted by a 300° K blackbody into an infrared spectrophotometer whose field-of-view it fills can be calculated. If the effective aperture of the spectrophotometer is f/2 or better and if the radiation detector is a typical thermal detector, then a bandwidth of 1 wavenumber at 600 wavenumbers (17 microns) should provide an output of the order of 10 microvolts (neglecting absorption in the spectrophotometer and in the air). It should be possible therefore to measure the emitted radiation of materials at ambient temperature directly in this region, provided suitable cooled shields are used to lower the surrounding background radiation. A simpler approach is to heat the sample of material under investigation to several hundred degrees C above ambient temperature.

*Unpublished data obtained by J. J. Triolo, Goddard Space Flight Center.

Integrated Emitted Radiation Measurements, for $\bar{e}$ (A 2 b)

The measurement problems are simplified in this case, compared with those of the preceding section (A 2 a), since spectral resolution is not required. Commercial radiometers are available to measure the emittance of materials to within 0.03 absolute* if the material's temperature is accurately known.

Thermal Methods

Equilibrium Thermal Measurements with Electrical Heating, for $\bar{a}$ (B 1 a)

If a sample of the test material is placed in a vacuum chamber that is then evacuated to 10^{-4} mm Hg or better, the sample can lose heat only by radiation to the walls of the chamber or by conduction through attached lead wires. If the walls of the vacuum chamber are essentially black and isothermal and if electrical heating leads are attached to an internally mounted heating element in the sample, the sample emittance can be calculated provided the wall temperature, sample temperature, sample surface area, electric power input to the sample, and the lead losses are known. Materials of low emittance require samples of large surface area to produce a sufficiently large ratio of radiative heat transfer to conductive heat transfer through the leads.

Equilibrium Thermal Measurements with Solar Simulator as Heater, for $\bar{a}/\bar{e}$ (B 1 b)

A sample of material suspended in a vacuum chamber evacuated to at least 10^{-4} mm Hg, and illuminated by a solar simulator of known intensity of illumination, will reach an equilibrium temperature T_2 given by the following equation:

$$T_2^4 = \left(\frac{\bar{a}}{\bar{e}}\right)\left(\frac{I}{\sigma}\right)\left(\frac{A_p}{A_s}\right) + T_1^4 \quad , \tag{11}$$

where

$\bar{a}$ = average solar absorptance of the sample's illuminated area (this will depend on the sample's shape – i.e., whether it is plane, spherical, cylindrical, etc. – and on the direction of illumination with respect to the axes of symmetry of the sample),

$\bar{e}$ = average thermal emittance of the sample,

I = intensity of illumination of the solar simulator – i.e., its total radiant power per unit area,

σ = Stefan-Boltzmann constant (5.67×10^{-12} watt/cm^2-°K),

A_p = projected area of the sample as viewed in the direction of illumination,

A_s = total surface area of the sample,

T_1 = temperature in degrees Kelvin of the vacuum chamber's walls.

*E.g., the Barnes R-4DT Industrial Radiometer (made by the Barnes Engineering Co., Stanford, Conn.).

It should be noted that the walls of the vacuum chamber are assumed to be black (for thermal radiation) and isothermal. The ratio of A_p/A_s is:

1/2 for a plane figure illuminated normally,

1/4 for a sphere, and

$1/2\left(1 + \frac{L}{R}\right)^{-1}$ for a cylinder illuminated on its axis, etc. (L is the length, and R the radius).

If the sample has a thermocouple attached to measure T_2, if thermocouples are also attached to the interior walls of the vacuum chamber to measure T_1, and if a calibrated thermal radiation detector is used to measure the intensity I of illumination from the solar simulator at the samples, then measurement of the sample's physical dimensions provides values for A_p and A_s, and all quantities are known in Equation 11 except $\bar{a}/\bar{e}$, which can therefore be determined. (For example, if $\bar{a}/\bar{e} = 1$, $T_1 = 0$, $I = 0.1397$ watt/cm² (the solar constant), then $T_2 = 60.3°$ C or $333.5°$ K for a flat plate illuminated normally.) Lead losses have been neglected in Equation 11.

Equilibrium Thermal Measurements with a Solar Simulator as Heater, Conductive Transfer Predominant, for $\bar{a}$ (B 1 c)

In this type of measurement no vacuum chamber is necessary. Radiation from a powerful solar simulator is allowed to illuminate a portion of the upper surface of a water-cooled, cylindrical hollow chamber. If the illuminated area is coated with a material whose solar absorptance is to be measured, then measurement of

1. The average radiant intensity of the solar simulator across the test surface,
2. The input and output temperatures of the cooling water,
3. The rate of flow of the cooling water, and
4. The area of the test surface illuminated

allows the solar absorptance of the test material to be computed. This method requires a sufficiently rapid flow of water to restrict the rise in output temperature of the cooling water to a value that is capable of precise measurement (say, 10° to 20° C) but that is not so large that radiative heat transfer or air conduction dissipates a significant portion of the input power absorbed by the illuminated test surface.

Dynamic Thermal Measurements with a Solar Simulator as Heater, for $\bar{a}$ and $\bar{e}$ (B 2 a)

A test sample coated with the material under investigation is suspended in a vacuum chamber evacuated to below 10^{-4} mm Hg. The vacuum chamber has cooled black walls (liquid-nitrogen cooling is desirable) except for a small port covered by a quartz window. The temperature of the test sample and the wall temperature are continuously monitored during the measurement process. The sample is first heated-up to 20° to 40° C above ambient temperature by the illumination of a solar simulator, incident upon the sample through the quartz window. The solar simulator is then turned *off*, and the sample is allowed to cool down to 20° to 70° C below ambient temperature. The radiant intensity of the solar simulator, at the sample, is continuously monitored during the heat-up phase of this

procedure. The rate of change of sample temperature with time dT/dt is obtained from the recorded curve of temperature as a function of time. The rate of change values are then plotted against T^4. If the solar simulator intensity and the wall temperature of the vacuum chamber remained approximately constant during the measurements, the data when plotted in this manner will fall on two parallel straight lines. All heat-up data will fall on (or near) one line, and the cool-down data will fall on the other line. If the thermal emittance of the material being measured is independent of its temperature and if the specific heat of the sample is also independent of temperature, then – as Gordon has shown (Reference 6) – the equation connecting dT/dt and T^4 during heat-up is

$$mc \frac{dT}{dt} = A_p \bar{a} I + P - A_s \bar{e} \sigma T^4 , \tag{12}$$

where all the quantities have been previously defined except

m = mass of sample,

c = specific heat of the sample per unit mass,

P = incident thermal radiation (from the walls of the vacuum chamber and the quartz window).

During cool-down, the solar simulator is turned *off* and Equation 12 reduces to

$$mc \frac{dT}{dt} = P' - A_s \bar{e} \sigma T^4 , \tag{13}$$

where P' is the incident thermal radiation for the cool-down. Equations 12 and 13 thus show that dT/dt plotted against T^4 produces two straight lines as follows:

Heat-Up (Solar Simulator *on*)

Slope of line,

$$s_H = - \frac{A_s \sigma}{mc} \bar{e} ; \tag{14}$$

Intercept with x axis,

$$\frac{dT}{dt} = 0 , \quad i_H = \frac{A_p \bar{a} I + P}{A_s \bar{e} \sigma} . \tag{15}$$

Cool-Down (Solar Simulator *off*)

Slope of line,

$$s_c = \frac{-A_s \sigma}{mc} \bar{e} ; \tag{16}$$

Intercept with x axis,

$$\frac{dT}{dt} = 0 \quad , \quad i_c = \frac{P'}{A_s \bar{e} \sigma} \quad . \tag{17}$$

It is seen therefore that the slope of both lines is proportional to $\bar{e}$ and that, if $P' = P$, the difference in the intercepts $i_H - i_c$ is proportional to $\bar{a}/\bar{e}$. Thus both $\bar{a}$ and $\bar{e}$ can be found by this method.

The advantage of this method, compared with equilibrium methods, is that measurements can be made more rapidly since equilibrium need not actually be achieved. Furthermore, since the values of $\bar{e}$ obtained by this method are based on the *slope* of a line relating dT/dt to T^4, rather than its *position* in the x-y plane, *constant* heat losses or heat inputs do not affect the measurements. Also, since the walls of the vacuum chamber are cooled, the incident thermal radiation is small compared with the solar simulator radiation, and uncertainties as to wall temperature or thermal radiation from the quartz window do not affect the measured value of $\bar{a}/\bar{e}$ too greatly.

Two technicians are required to operate the equipment used for measuring $\bar{a}$ and $\bar{e}$ by the above method at Goddard Space Flight Center (GSFC), one to operate the solar simulator (a carbon arc lamp with rare-earth cored carbons) and the other to operate the vacuum chamber and temperature recorder. About 2 to 3 days are required for each complete measurement of the $\bar{a}$ and $\bar{e}$ values of a material; this includes time required to pump down the vacuum chamber and time required to reduce the temperature data.

Dynamic Thermal Measurements with Adiabatic Cooling for $\bar{e}$ (B 2 b)

This method is similar to (B 2 a) above, but in this case the light source need not be a solar simulator since it is used solely to heat the test sample to a temperature somewhat *above* the temperature at which the thermal emittance value is desired. Furthermore, the intensity of the light source is not measured, and the walls of the vacuum chamber need only be cooled to a temperature appreciably *less* than the temperature at which $\bar{e}$ is desired. A description of this method is given by Butler and Inn (Reference 7).

DESCRIPTION OF GSFC EQUIPMENT FOR MEASURING SPACECRAFT COATING $\bar{a}$ AND $\bar{e}$ BY DYNAMIC THERMAL VACUUM TECHNIQUES (WITH A SOLAR SIMULATOR)

The apparatus has five main components:

1. The vacuum system,
2. The solar simulator,
3. The liquid-nitrogen-cooled shroud (which goes inside the vacuum bell jar),
4. The temperature recorder, and
5. The solar simulator intensity measuring equipment.

All five components are commercially available. The *vacuum system* is a High Vacuum Equipment Corp.* C0018 (18-inch-diameter) Bell Jar Evaporator. This system (without the liquid-nitrogen-cooled shroud) has an ultimate vacuum of approximately 5×10^{-7} mm Hg. The bell jar is stainless steel with two 5-inch-diameter quartz sight ports, as shown in Figure 1 (only one port is used for the measurements however).

The *solar simulator* is a Strong Electric Co.† "UHI" Automatic Reflector Arc Lamp, type 91013-1W/0, which operates at about 60 volts and 175 amperes input to the lamp itself. The arc lamp uses 13.6 mm cored carbons for both the positive and negative carbons. The negative carbon is copper-shielded. The arc will operate automatically for about 45 minutes on one positive carbon.

*High Vacuum Equipment Corp., Hingham, Mass.
†The Strong Electric Corp., Toledo, Ohio.

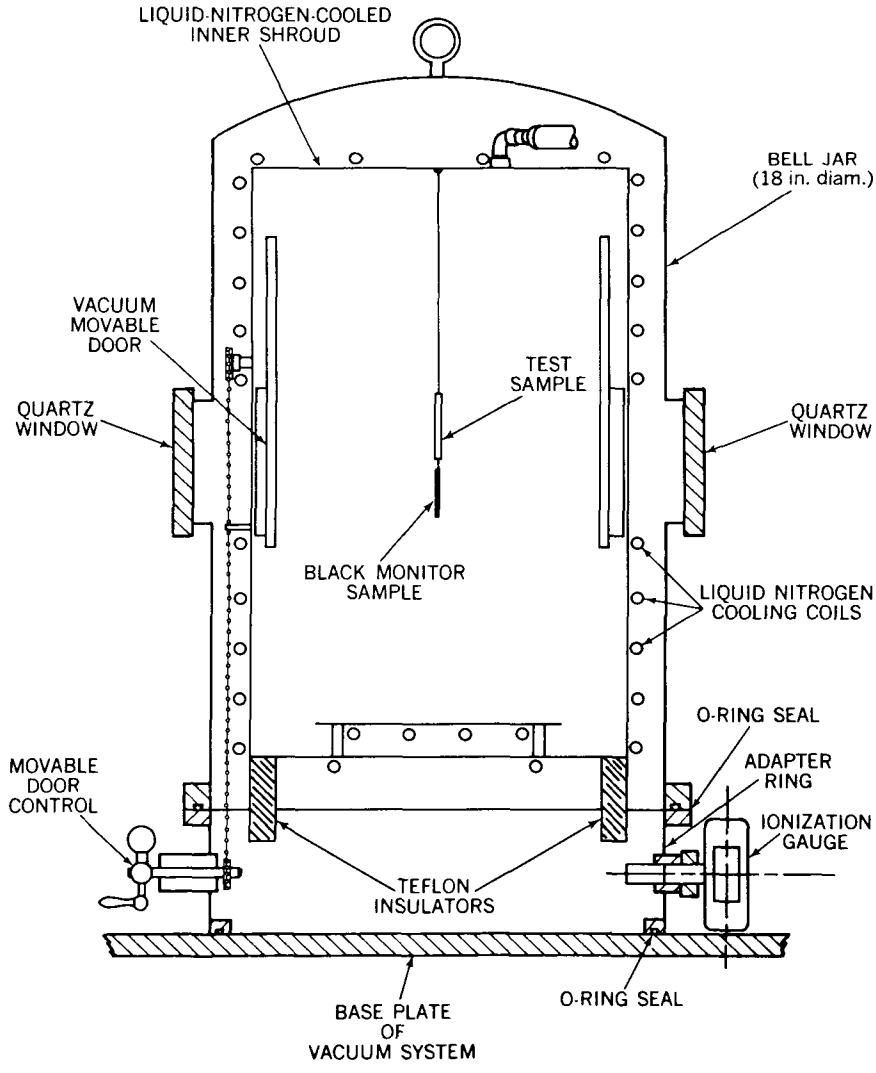

Figure 1—Cross section of the cooled shroud and vacuum system bell jar.

The *liquid-nitrogen-cooled shroud* (Figure 2) was also designed and made by the High Vacuum Equipment Corp. It is 15 inches in diameter, 24 inches high, and is designed – as Figure 1 shows – to fit inside the bell jar of the vacuum system except for the shroud base, the "adapter ring," which rests on the baseplate of the vacuum system and supports the bell jar. The shroud is made of nickel-plated copper and has two circular 5-inch-diameter ports, one of which has a cover that is externally movable through a chain attached to a rotary crank handle in the adapter ring (Figures 1 and 3). The shaft of the crank handle penetrates the adapter ring through a vacuum seal fitting. The other port has a cover that can be moved, but has no external handle. The upper portion of the shroud opens up about a vertical hinge like a "clam shell" for the insertion of test samples (Figure 2). The adapter ring also contains the liquid nitrogen feed-throughs, the thermocouple feed-throughs, and the vacuum seal for the ionization gauge (Figure 3). The adapter ring serves the purpose of lifting the base of the shroud so that it does not obstruct the upward movement of the high vacuum valve, located in the baseplate of the vacuum system. The bottom of the adapter ring is joined to the baseplate by an O-ring seal, and the adapter ring top is joined to the bottom of the bell jar by an O-ring seal.

The *temperature recorder* (Figure 4) is a Minneapolis-Honeywell Universal Model 15 "Electronik" multipoint recorder,* with a temperature range of -200° to +100° C. It records

*Minneapolis-Honeywell Regulator Co., Brown Instrument Div., Philadelphia, Pa.

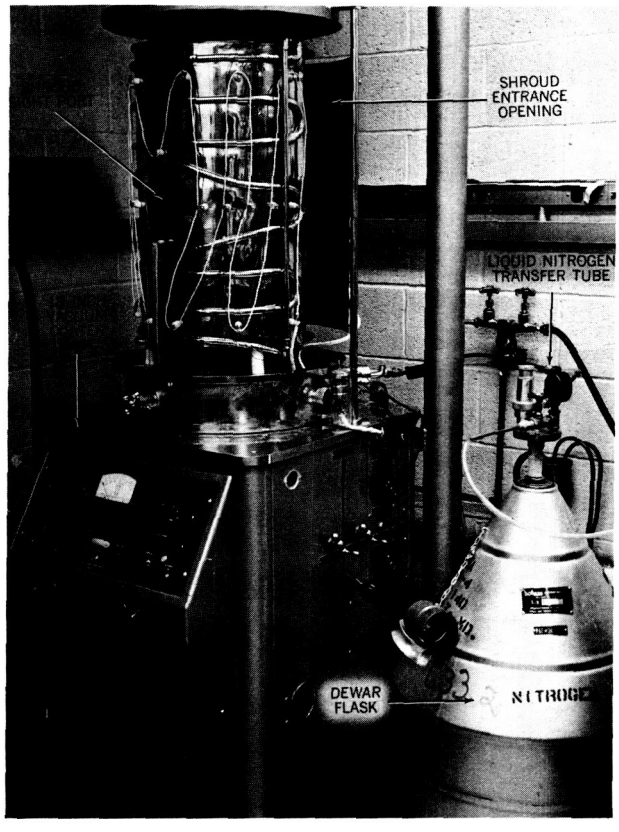

Figure 2—The vacuum system and cooled shroud, with shroud and movable door in the "open" position.

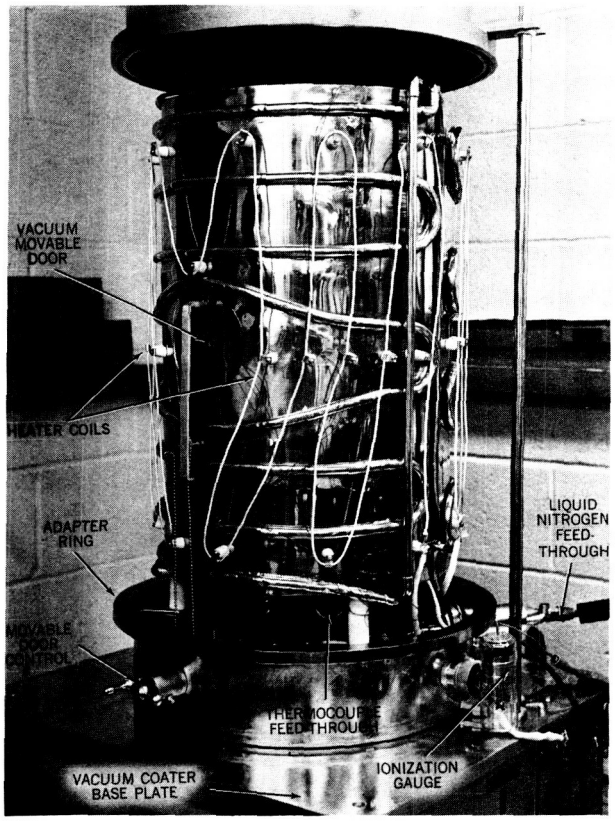

Figure 3—Cooled shroud detail showing thermocouple leads and feed-throughs.

Figure 4—The complete thermal vacuum setup showing solar simulator (carbon arc), light intensity measuring equipment, and multichannel temperature recorder. Bell jar is in the "operating" position.

a temperature every 2 seconds; and, since there are eight channels, data points are recorded 16 seconds apart for any particular channel.

The *solar simulator intensity measuring equipment* (Figure 4) consists of an Eppley Laboratory Pyrheliometer, 50 junction,* as the detector, and a Hewlett-Packard Microvoltmeter Model 425A† to indicate the detector output.

The liquid nitrogen feeding mechanism is also important and includes a 50 liter Dewar flask with a transfer tube driven by dry nitrogen (see Figure 2).

The light from the solar simulator is collimated by a quartz lens, plano-convex, 6 inches in diameter with a focal length of 23 inches (Figure 5). This lens collimates the light from the solar simulator to within 12 degrees. (This is due to the fact that light is utilized from both the positive carbon crater and the tail flame, which is 2 to 3 inches in length.) In use, the carbon arc lamp is placed so that the arc gap is located 95 inches from the test sample, which is suspended in the center of the shroud.

*The Eppley Laboratory, Inc., Newport, R. I.
†Hewlett-Packard, Palo Alto, Calif.

A motor-driven chopper is placed between the collimating lens and the vacuum chamber. Since the light intensity at the sample is too high–about 2 solar constants–when the carbon arc lamp is operating at its level of maximum stability, the chopper is required to reduce this light intensity to the desirable level of 1 solar constant while the carbon arc lamp operates at its optimum output level. The chopper has interchangeable blades that attenuate the light beam by different proportions.

The test samples used with this equipment are made in a "sandwich" form. Two copper plates, 2 inches square by 1/32 inch thick, are accurately cemented together with a 5 mil copper-constantan thermocouple centered between them (see Figure 6). To make this "sandwich," the plates are held in place by a jig to keep the thermocouple in position and to line up the square edges of the plates. An epoxy cement* is used to bind the two halves of the "sandwich" together. The thermocouple junction is forced into good thermal contact with both copper plates by mechanical pressure; the epoxy cement locks the thermocouple in place and maintains the good thermal contact. A mold release compound called "PVA"† is used to prevent the cement from adhering to the jig; this mold release compound, unlike grease, leaves no residue to prevent the test coating from adhering to the copper substrate. At this point the coating to be measured is applied to the copper sandwich. Coating after the assembly is cemented together prevents the high emittance epoxy from remaining uncoated and thus producing a large error for low emittance coatings (like polished or evaporated metals). In addition, when evaporated metal coatings are to be measured, the coating is allowed to extend onto the thermocouple leads also; this has the effect of reducing the error due to heat loss through the leads. If the coating has a high emittance,

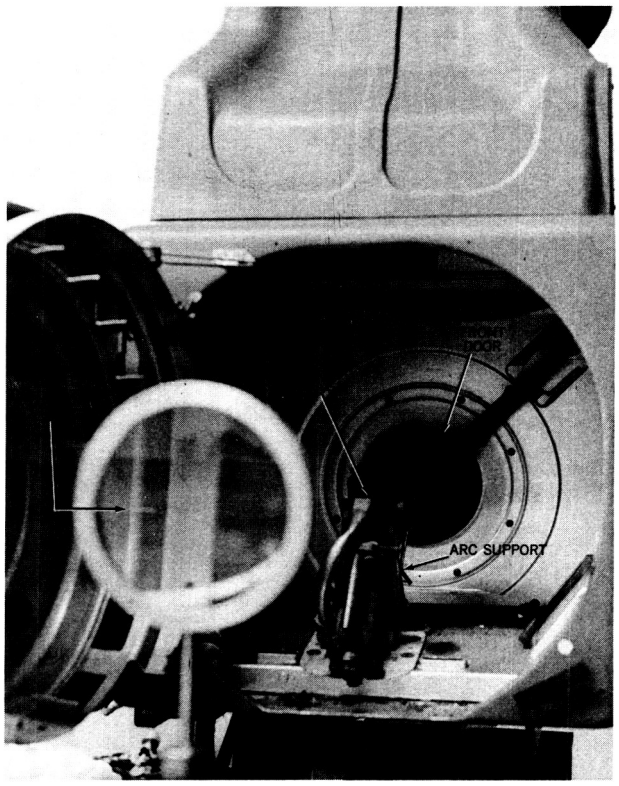

Figure 5—Solar simulator detail showing the quartz collimating lens and the positive and negative carbons.

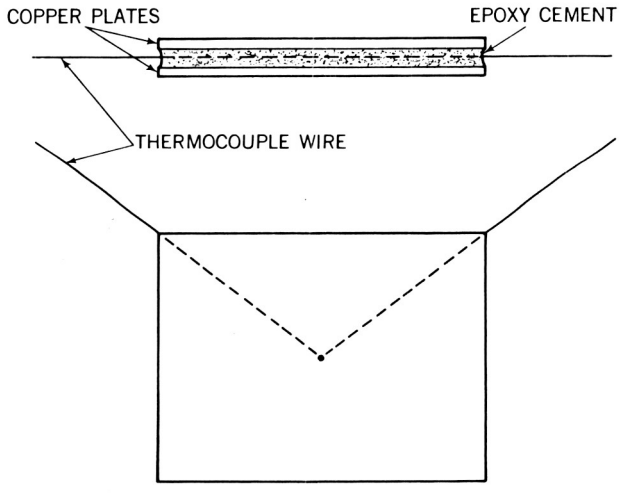

Figure 6—Test sample thermocouple configuration.

*"Twin Weld," manufactured by Fybraglas Industries, Chicago 13, Ill.
†Polyvinyl Alcohol (PVA), Gilbert Plastics, 4300 E. Monument St., Baltimore, Md.

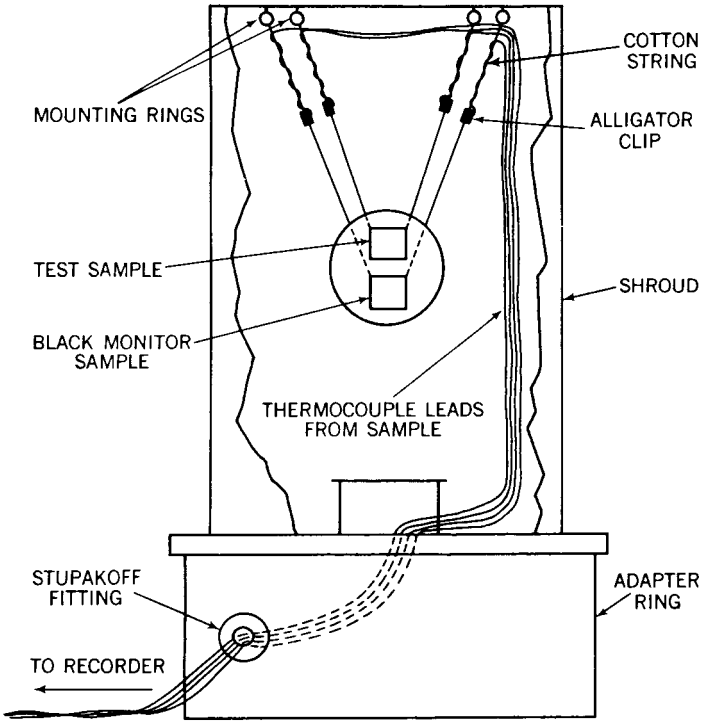

Figure 7—Sample suspension technique and thermocouple vacuum feed-throughs.

the enamel is stripped off the thermocouple leads, leaving 3 inches of bare thermocouple wire, which has an emittance of less than 0.1.

The sample assembly is suspended from the top of the shroud by means of its thermocouple leads, as shown in Figure 7. The leads are led into the vacuum system by means of a Stupakof fitting located in the adapter ring. Thus the thermocouple wires are a continuous stretch of one metal only from the recorder terminals to the sample, the Stupakoff fitting having an equal number of copper and constant lead-throughs. In this way stray thermal voltages, due to unequal temperature gradients between junctions of dissimilar metals, are avoided.

OPERATING PROCEDURE FOR OBTAINING THERMAL EMITTANCE MEASUREMENTS WITH THE GSFC THERMAL VACUUM CHAMBER

The test samples are mounted in the shroud and, by adjusting the leads, are centered in the sight port. A small battery-powered incandescent light is placed at the arc crater position and is collimated to illuminate the samples. This enables the samples to be positioned so that their entire frontal area is illuminated. The wires are held in place with two alligator clips suspended from the top of the shroud interior by two lengths of cotton string (see Figure 7).

Next, the chamber is closed and pump-down is started. When the pressure is below 10^{-4} mm Hg, liquid nitrogen is circulated through the shroud, the recorder is turned *on*, and shroud temperature is monitored. The system is ready for operation when the shroud has dropped to about a -190° C stable temperature (at equilibrium, the shroud is uniform in temperature to within ±5° C). At this point the pressure is normally in the low 10^{-6} range. To reduce the errors due to heat loss from the sample caused by gas conduction, the measurement procedure is not started until about 1 hour later, when the pressure has reached the low 10^{-7} range (the ultimate vacuum of the GSFC system is 2×10^{-7} mm Hg, which is reached in 2-1/2 hours).

The movable door in the shroud is now closed so that the arc can be turned *on* – and adjusted after warmup – without illuminating the test sample prematurely. When the intensity is steady, as determined by the pyrheliometer (see Figure 4), the movable door is opened and the heat-up data are recorded. After the sample has traversed the desired temperature range, the movable door is closed and the arc lamp is turned *off*. The door remains closed until the arc carbons stop glowing. (The door is also closed during a heat-up run if the carbon arc lamp acts up and the intensity begins to wander.) For coatings having a high $\bar{a}/\bar{e}$ ratio, the motor-driven chopper is employed to reduce the arc lamp illumination striking the sample, and thus to bring the sample equilibrium temperature down to a value within the range of the recorder.

After the movable door is closed and the test sample is no longer illuminated by the carbon arc lamp, the sample starts to cool down. The sample temperature is also recorded during this cool-down process. The heat-up and subsequent cool-down cycle is repeated several times to increase the amount of data available and to improve the accuracy of the $\bar{a}$ and $\bar{e}$ values derived from these data by averaging a number of measurements of $\bar{a}$ and $\bar{e}$.

THE MAJOR ERRORS AFFECTING THE ACCURACY OF $\bar{a}$ AND $\bar{e}$ VALUES OBTAINED BY TRANSIENT THERMAL VACUUM TECHNIQUES

There are two types of errors to be considered: (1) random errors, and (2) systematic errors.

Random Errors

The random errors are the major accuracy limitation of the measurements made with the present equipment. Most of the systematic errors can be computed and corrected for, as is shown below. Random errors in the temperature and light intensity measurements *cannot* be corrected for, however, but the magnitude of these errors can be estimated. The fractional errors due to random errors were calculated to be as follows:

For thermal emittance values,

$$\frac{\Delta\bar{e}}{\bar{e}} = \pm 0.070.$$

For solar absorptance values,

$$\frac{\Delta\bar{a}}{\bar{a}} = \pm 0.075.$$

For $\bar{a}/\bar{e}$ values,

$$\frac{\Delta\left(\frac{\bar{a}}{\bar{e}}\right)}{\left(\frac{\bar{a}}{\bar{e}}\right)} = \pm 0.028.$$

These fractional errors can be reduced by averaging several measurements or by improving the instrumental accuracies (e.g., reduced noise) and the read-off accuracies. The assumptions made in calculating the fractional errors above are:

1. $\sigma T^4 >> \sigma T_0^4$ (i.e., sample equilibrium temperature with *no* illumination is much lower than ambient temperature),
2. Measurements for $\bar{a}/\bar{e}$ are made near the sample equilibrium temperature *with* illumination,
3. The error in time measurement is negligible, and
4. The spectral match of the solar simulator with the solar spectrum is perfect.

Systematic Errors

The systematic errors are due to the following causes:

1. Thermal conduction losses through the leads,
2. Variation of thermal emittance with temperature,
3. Variation of specific heat of the substrate (copper) with temperature,
4. Heat loss due to gas conduction, and
5. Temperature gradients within the test sample.

After a brief calculation the approximate solution of the fifth source seems to be negligible. Each of the other four sources of error will now be examined in detail.

Heat Loss Due to Thermal Conduction Through the Leads

Gordon (Reference 6) gives the following equations for the heat flow through a lead wire:

$$q = \pi \left[\frac{K\sigma \bar{e}_w D^3 \left(T^5 - 5T_0^4 T + 4T_0^5 \right)}{10} \right]^{\frac{1}{2}} , \tag{18}$$

where

q = heat flow through the lead wire,

K = thermal conductivity of the wire,

$\bar{e}_w$ = thermal emittance of the wire,

D = diameter of the wire,

T = sample temperature,

T_0 = temperature of the vacuum chamber wall.

The derivation of this equation also has been worked out by Gordon.* It starts from the fundamental differential equation describing the heat flow:

$$K \frac{d^2\theta}{dx} \pi r_w^2 = \bar{e}_w \sigma \left(\theta^4 - T_0^4\right) 2\pi r_w , \tag{19}$$

where

θ = temperature along the wire,
r_w = radius of the wire,
x = distance along the wire measured from the sample.

Then, by one integration, Gordon proceeds efficiently to Equation 18. The wire is assumed to be semi-infinite, of isothermal cross section, so that the temperature is a function only of x; the heat flow is assumed to be steady state. The boundary condition at $x = \infty$ is $T = T_0$ and $d\theta/dx = 0$.

Gordon further – in Reference 6 – compares the heat flow through the lead wire with the radiative heat flow from the sample. He gives an upper bound for the fractional error in $\bar{e}$, the thermal emittance of the test sample, as:

$$\frac{\pi}{A_s \bar{e}} \left(\frac{K \bar{e}_w D^3}{10 \sigma T^3}\right)^{\frac{1}{2}} \geq E , \tag{20}$$

where E is the fractional error in e, and A_s is the surface area of the test sample.

A typical numerical example for a low emittance sample is:

K = 0.97 cal/sec - cm-°K (copper at 300°K)
$\bar{e}_w$ = 0.04 (copper, 300°K)
D = 0.005 in. = 0.0127 cm
T = 300°K
σ = 5.67×10^{-5} erg/cm^2 -sec-°K^4
A_s = 54.8 cm^2 (2 x 2 x 1/16 in.)
$\bar{e}$ = 0.02 (vacuum-deposited gold)

Inserting the above values in Equation 20 gives an upper bound for the fractional error in $\bar{e}$ due to lead losses of 0.04. (The lead loss for the constantan lead of the copper-constantan thermocouple is negligible compared with the lead loss for the copper lead because of the much lower relative thermal conductivity of constantan compared with copper.) The fractional error in $\bar{e}$ is defined as $\Delta\bar{e}/\bar{e}$, where $\Delta\bar{e}$ is the absolute error in $\bar{e}$. For samples possessing a higher thermal emittance, the fractional lead loss error given by Equation 20 will be proportionately less, of course.

*Private communication with G. E. Gordon.

The Variation of Thermal Emittance with Temperature (Applies to Metals Only)

Jakob (Reference 5, p. 51) has shown that the thermal emittance of polished metals varies with the temperature. This is due to two factors:

1. The variation in the spectral emittance with wavelength, which is of the form

$$e_\lambda = 0.476 \left(\frac{r_e}{\lambda}\right)^{\frac{1}{2}} - 0.148 \frac{r_e}{\lambda} , \tag{21}$$

where e_λ is the spectral emittance at wavelength λ and r_e is the electrical resistivity (cgs units). (Equation 21 holds for $0<r_e/\lambda<0.5$.)

2. The variation in the electrical resistivity with temperature. For pure metals (Reference 5, p. 45) the resistivity is approximately proportional to the absolute temperature. From Equation 21 it is obvious that, as the temperature increases and the maximum of the Planck blackbody spectrum shifts towards shorter wavelengths in accordance with Wien's law (Reference 4, p. 434), the emittance will increase. Integration of Equation 21 over the blackbody spectrum to obtain the total thermal emittance at a temperature of T degrees absolute yields

$$\bar{e} = 0.751 \left(r_e T\right)^{\frac{1}{2}} - 0.396\ r_e T . \tag{22}$$

(Equation 22 holds for $0 < r_e T < 0.2$.)

For the region of interest, that is, for measurements of the thermal emittance of metals near ambient (300°K) temperature, a typical value of $r_e T$ is 7.5×10^{-4} (cgs) for gold.

To consider the effect of the variation of the thermal emittance with temperature on the measured value of $\bar{e}$ computed from the slope – or tangent, if not a straight line – of the curve connecting values of dT/dt with values of T^4, it is desirable to repeat Equation 12 for the heat-up curve of the sample:

$$mc \frac{dT}{dt} = A_p \bar{a} I + P - A_s \bar{e} \sigma T^4 . \tag{12}$$

Let

$$\frac{dT}{dt} \equiv y ,$$

$$T^4 \equiv x ,$$

$$mc \equiv c' ,$$

$$A_s \sigma \equiv \sigma' .$$

Using these substitutions, Equation 12 reduces to

$$c'y = A_p \bar{a} I + P - \sigma' \bar{e} x \,. \tag{23}$$

The tangent to the above curve at the point (y, x) is $dy/dx \equiv y'$, and

$$c'y' = -\sigma' \bar{e} - \sigma' \bar{e}' x \,, \tag{24}$$

where

$$\bar{e}' \equiv \frac{d\bar{e}}{dx} \,.$$

To evaluate $\bar{e}'$ in terms of $d\bar{e}/dT$ and dT/dx, since

$$\frac{d\bar{e}}{dx} = \frac{d\bar{e}}{dT} \cdot \frac{dT}{dx} \,,$$

it is necessary to return to Equation 22. This equation reduces to

$$\bar{e} = 0.751 \left(r_e T\right)^{\frac{1}{2}} \tag{25}$$

for metals near ambient temperature. Equation 25 may be written in the form

$$\bar{e} = \bar{e}_0 \frac{T}{T_0} \tag{26}$$

since – as mentioned above –

$$r_e \approx r_{e,0} \frac{T}{T_0} \,, \tag{27}$$

where $\bar{e}_0$ is the value of $\bar{e}$ at temperature T_0, and $r_{e,0}$ is the value of r_e at T_0.

By Equation 26 therefore,

$$\frac{d\bar{e}}{dT} = \frac{\bar{e}_0}{T_0} \,; \tag{28}$$

and so

$$-c'y' = \frac{5}{4} \sigma' \bar{e} \tag{29}$$

or

$$\bar{e} = -\frac{4}{5} \left(\frac{c'y'}{\sigma'}\right). \tag{30}$$

On the other hand, assuming that $\bar{e}$ is *not* a function of T leads to the result:

$$\bar{e} = -\left(\frac{c'y'}{\sigma'}\right). \tag{31}$$

Thus the value of $\bar{e}$ obtained by Equation 31 must be multiplied by 4/5 to correct for the variation of $\bar{e}$ with T if the sample coating is a pure metal. (Obviously the correction factor depends on the exponent of the power of T that best describes the variation of $\bar{e}$ with T for the test material, even if it is not a pure metal.)

The Variation of Sample Specific Heat (Copper) with Temperature

The specific heat of copper varies quite rapidly with temperature from 0°K to about 300°K (Reference 8). From 300°K to higher temperatures, it increases linearly at a rate of roughly 0.01 cal/gm-°K per every 370°K. At 300°K the specific heat of copper is approximately 0.093 cal/gm-°K.

If both c' and $\bar{e}$ are considered as functions of T in Equation 13, then differentiating y with respect to x shows that

$$y\left(\frac{dc'}{dx}\right) + \left(\frac{dy}{dx}\right) c' = -\sigma'\bar{e} - \sigma'\left(\frac{d\bar{e}}{dx}\right) x$$

or

$$y\left(\frac{dc'}{dx}\right) + \left(\frac{dy}{dx}\right) c' = -\frac{5}{4}\sigma'\bar{e} \quad , \tag{32}$$

where some of the substitutions of the preceding section have been employed. We assume next that P' in Equation 13 can be neglected, and we substitute the resulting value of y into Equation 32 to get

$$-\frac{\sigma'\bar{e}x}{c'}\left(\frac{dc'}{dx}\right) + c'\left(\frac{dy}{dx}\right) = -\frac{5}{4}\sigma'\bar{e} \quad .$$

Therefore, solving for $\bar{e}$ leads to the result

$$\bar{e} = \frac{-c'\left(\frac{dy}{dx}\right)}{\sigma'\left[\frac{5}{4} - \left(\frac{x}{c}\cdot\frac{dc}{dx}\right)\right]} . \tag{33}$$

For the linear portion of the curve giving the specific heat of copper as a function of temperature, we found that $(x/c')(dc/dx) = 0.022$, approximately. This is much less than 5/4, and so the variation of specific heat of copper with temperature is insignificant above 300°K but begins to be significant below 200°K.

Heat Losses Due to Thermal Conduction Through the Residual Gas in the Vacuum Chamber

The fractional error E in $\bar{a}/\bar{e}$ due to thermal conduction through the gas in the vacuum chamber is given by Gordon (Reference 6) as

$$E < \left(\frac{3}{2}\right) \frac{K\left(T - T_0\right)\nu}{\bar{e}\sigma\left(T^4 - T_0^4\right)} < \left(\frac{3}{2}\right) \frac{K\nu}{\bar{e}\sigma T^3} , \tag{34}$$

where

K = Boltzmann constant (1.38×10^{-16} erg/deg),

ν = number of molecules that impinge on unit area of the sample in unit time (about 1.3×10^{23} cgs for air at S.T.P.),

T_0 = temperature of the vacuum chamber wall (°K),

T = sample temperature;

and it is assumed that the average energy transfer per molecule is not greater than 3/2 $K(T - T_0)$. This error is negligible at pressures in the 10^{-7} range, even with emittances as low as 0.01, for temperatures above 100°K. Even at very low temperatures near 100°K, the proportional error for an emittance of 0.01 and a pressure of 2×10^{-7} mm Hg will be only about 0.012.

DATA REDUCTION PROCEDURE

As mentioned in the section on dynamic thermal measurements (p. 9), the values of $\bar{e}$ and $\bar{a}/\bar{e}$ can be calculated by using Equations 14 through 17, so that

$$s_H = s_c = \frac{-\sigma A_s \bar{e}}{mc}$$

and

$$i_H - i_c = \frac{A_p \bar{a} I + P}{\sigma A_s \bar{e}} - \frac{P'}{\sigma A_s \bar{e}} .$$

(The above symbols were defined with the referenced equations.)

If it is assumed that the errors previously mentioned have been corrected for, or found negligible, and if it is further assumed that $P = P'$ [i.e., that the absorbed thermal power from the surroundings

(specifically *excluding* the radiation from the solar simulator) is equal for both the heat-up and cool-down phases of the measurement], then

$$\bar{e} = \frac{-s_c mc}{A_s \sigma} = \frac{-s_H mc}{A_s \sigma} \tag{35}$$

and

$$\frac{\bar{a}}{\bar{e}} = (i_H - i_c) \frac{\sigma A_s}{I A_p} \quad . \tag{36}$$

Note that, if dT/dt is plotted against σT^4 instead of T^4, the σ drops out of Equations 35 and 36.

The data are recorded by the multipoint recorder in the form of temperature as a function of time. The intensity of the solar simulator is measured by the pyrheliometer and the microvoltmeter. A smooth curve is run through the temperature-time data so that the "noise" can be eliminated; the slope (or tangent) is read from this curve at desired intervals. "Ship's curves" are very useful for the curve-fitting process. The time interval chosen varies inversely with the rate of temperature change; for instance, this interval near equilibrium (dT/dt very small) is as long as 640 seconds for samples coated with vacuum-evaporated metals of low emittance.

Tables of σT^4 in watts/cm^2 are employed — the values of T running from 0° to 600°K in 0.1 degree intervals — and are found to expedite the calculations. The tables can easily be run off on an IBM digital computer such as the 7090. Since the heat-up and cool-down lines on the graph of dT/dt versus σT^4 are usually parallel (i.e., if the surroundings remain at a constant temperature, the lines are parallel), the emittance can be calculated from either line. The cool-down line, however, has more data points (since dT/dt is less in absolute value for the cool-down curve than it is for the heat-up curve) and hence is more reliable for this reason.

After uncorrected values of $\bar{e}$ and $\bar{a}$ have been obtained in this manner, the four systematic errors previously listed are calculated and the appropriate corrections are made.

Table 1 presents the results of some optical and thermal vacuum measurements made by the Thermal Systems Branch at GSFC. Conversion factors for converting total normal emittance (from optical measurements) to total hemispherical emittance (from thermal vacuum measurements), and vice versa, are given in Jakob's text on heat transfer (Reference 5, pp. 43, 51, and 52). For very low emittance metal coatings the ratio of total normal to total hemispherical emittance is, for example, about 1.3. For dielectrics having a total normal emittance of 0.9, the ratio is 0.935.

Figure 8 shows a typical plot of dT/dt versus σT^4 for carbon black silicone base paint. Some evaluation of the system can be made by noting the parallel lines and the cool-down intercept of the abscissa (near zero).

Table 1

Comparison of Solar Absorptance and Thermal Emittance Values, Obtained by Optical and Thermal Vacuum Measurements, for Four Common Spacecraft Coatings

Coating*	$\bar{a}$ and $\bar{e}$ Values†					
	$(\bar{a}/\bar{e})_H$	$\bar{e}_{\nu c}$	$\bar{e}_{NC}$	$\bar{e}_{NM}$	$\bar{a}_c$	$\bar{a}_{DK}$
Evaporated Gold	9.2	0.0239	0.015	--	0.195	0.200
Aluminized Mylar‡	2.68	0.0618	0.037	0.035	0.129	0.131
Evaporated Aluminum	4.02	0.0424	0.026	0.022	0.17	0.156
Carbon Black Paint, Silicon Vehicle	1.18	0.817	0.872	0.907	0.964	0.956

*Vacuum-deposited metals, and paint.

†Where $(\bar{a}/\bar{e})_H$ = ratio of solar absorptance to total normal emittance (for T = 300°K),

$\bar{e}_{\nu c}$ = uncorrected total hemispherical emittance as measured thermally,

$\bar{e}_{NC}$ = corrected total normal emittance calculated from thermally measured total hemispherical emittance,

$\bar{e}_{NM}$ = total normal emittance measured optically (should be close to $\bar{e}_{NC}$),

$\bar{a}_c$ = solar absorptance calculated from thermal measurements with a carbon arc solar simulator,

$\bar{a}_{DK}$ = solar absorptance calculated from optical measurements (should be close to $\bar{a}_c$).

‡With scribed lines 2 to 3 mils thick forming 1/4 in. squares of evaporated aluminum.

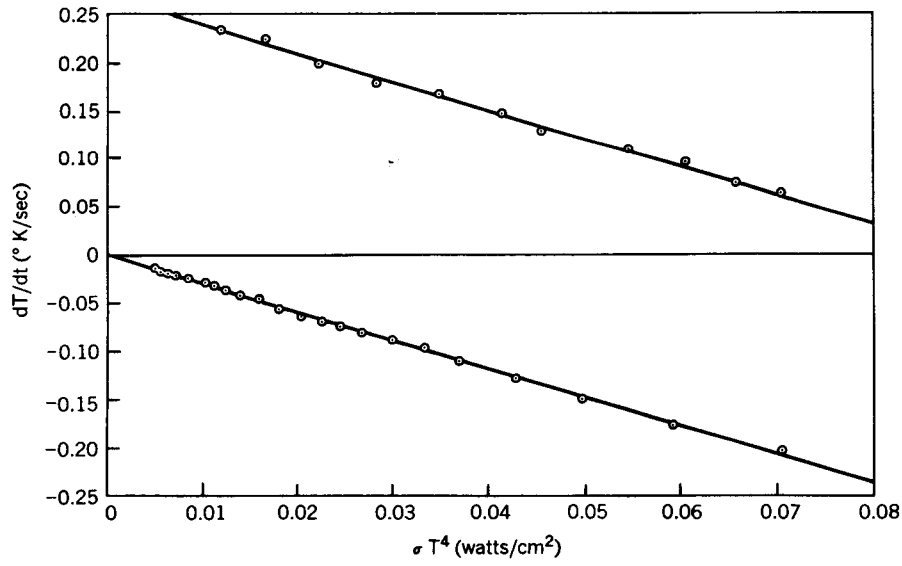

Figure 8–Typical data for derivative of temperature with respect to time dT/dt vs. σT^4 (σ is the Stefan-Boltzmann constant) for carbon black in silicone vehicle paint.

CONCLUSIONS

The accuracy of the measured $\bar{a}/\bar{e}$ ratio is probably less than that predicted in the section on major errors, p. 17, since the spectral match of the solar simulator (carbon arc lamp) with the solar spectrum is not exact. (A project for future investigation will be to measure the spectral distribution of the carbon arc as a function of the current and intensity.)

The accuracy of the thermal emittance measurement is especially good for low emittance materials, compared with the accuracy of the optical and thermal equilibrium methods of measuring $\bar{e}$ for these materials. Therefore this type of measurement fills a need even though it consumes more man-hours of labor than the optical method by a factor of perhaps 2 – since one thermal vacuum measurement requires about 6 man-days.

All the emittance data in Table 1 are within the accuracy predicted in the section on major errors. The accuracy can be improved by increasing the accuracy of the temperature measurement, probably by using a manually balanced potentiometer bridge to measure the thermocouple voltages.

FUTURE IMPROVEMENTS AND MODIFICATIONS

Improvements and modifications to the present equipment planned for the near future are the following:

1. A *multisample holder* that will permit more than one set of measurements for each pump-down of the vacuum system.

2. A *digital computer program* that will allow a good deal of the data reduction process (described in the section "Data Reduction Procedure") to be done by a computer. It is estimated that this computer program will reduce the number of man-days consumed in data reduction for each measurement from 3 man days to 0.5! Initially the data will be acquired from the multipoint recorder chart and reproduced on punched cards suitable for one of GSFC's IBM 7090 Digital Computers. Eventually, it is planned to digitalize the output of the multipoint recorder and then feed this digital output directly to a computer.

3. An *oil-free vacuum system* that will eliminate the possibility of oil from the diffusion pump backstreaming onto the test sample. At present, backstreaming is prevented by continuously running liquid nitrogen through the shroud and baffle; when the liquid nitrogen is not used, test samples quickly (in less than 1 day) become contaminated with oil. This oil-free vacuum system will employ a conventional mechanical forepump coupled with a Welch "Turbo-Molecular" pump,* which works on the molecular-drag principle (Reference 9). Although this type of pump uses no oil except for lubrication, a cooled baffle or trap probably will be useful here. The oil-free vacuum system will also eliminate the possibility of a diffusion pump "boiling over" because of the failure of the cooling water.

*Welch No. 1377A Turbo-Molecular Pumping System, made by the Welch Scientific Co., Chicago 10, Ill.

REFERENCES

1. Hass, G., Drummeter, L. F., and Schach, M., "Temperature Stabilization of Highly Reflecting Spherical Satellites," *J. Opt. Soc. Amer.* 49(9):918-924, September 1959.
2. Johnson, F. S., "The Solar Constant," *J. Meteorol.* 11(6):431-439, December 1954.
3. Jacquez, J. A., and Kuppenheim, H. F., "Theory of the Integrating Sphere," *J. Opt. Soc. Amer.* 45(6):460-470, June 1955.
4. Jenkins, F. A., and White, H. E., "Fundamentals of Optics," 3rd Ed., New York: McGraw-Hill, 1957, pp. 531, 208, 429, and 434.
5. Jakob, M., "Heat Transfer," New York: Wiley, 1949, Vol. 1, pp. 41-52.
6. Gordon, G. D., "Measurement of Ratio of Absorptivity of Sunlight to Thermal Emissivity," *Rev. Sci. Instr.* 31(11):1204-1208, November 1960.
7. Butler, C. P., and Inn, E. C. Y., "The Total Hemispherical Emissivity of Metals," U. S. Naval Radiological Defense Lab., San Francisco, USNRDL-TR-327, May 28, 1959.
8. Goldsmith, A., Waterman, T. E., and Hirschhorn, H. J., "Thermophysical Properties of Solid Materials. Vol. 1-Elements (Melting Temperature Above 1000° F)," Rev. Ed., Armour Res. Found. WADC Tech. Rept. 58-476, Vol. 1, August 1960.
9. Becker, W., "Über Eine Neue Molekularpumpe," in: *Advances in Vacuum Science and Technology: Proc. 1st Internat. Congress on Vacuum Techniques, Namur, Belgium, June 1958,* ed. by E. Thomas, New York: Pergamon Press, 1960, Vol. 1, pp. 173-176.